Lappeenranta University of Technology
School of Engineering Science
Computational Engineering and Technical Physics
Technomathematics

Berk Aydın

FLIGHT TRACK INITIALIZATION FOR PASSIVE RADAR

Master's Thesis

Examiners: Dr. Tuomo Kauranne
Miika Tolonen

Supervisor: Dr. Tuomo Kauranne

ABSTRACT

Lappeenranta University of Technology
School of Engineering Science
Computational Engineering and Technical Physics
Technomathematics

Berk Aydın

Flight Track Initialization For Passive Radar

Master's Thesis

2018

33 pages, 23 figures, 1 table.

Examiners: Dr. Tuomo Kauranne
Miika Tolonen

Keywords: passive radar, track initialization, tracking, Kalman filter, nearest neighbor search

The present work presents a track initialization algorithm developed for a Passive Multistatic Radar using Doppler-only measurements. In absence of initial state, Kalman filters can diverge. In a passive multistatic radar system, these initial parameters cannot be calculated analytically. We first developed a curve tracking algorithm to determine the detected aircraft. Another algorithm was developed to estimate initial parameters based on nearest neighbor search. The performance of the algorithm was evaluated by simulations and observations.

PREFACE

I wish to thank my supervisor Dr. Tuomo Kauranne for suggesting me this interesting topic and his brilliant ideas.

I would like to thank Miika Tolonen for all his support and contribution to this work.

This work has been funded by MATINE, Scientific Advisory Board for Defence, Finland and Lappeenranta University of Technology. I wish to thank them for their support.

Finally I would like to thank to my parents and my long time friend Bora Atalay for their support.

Lappeenranta, August 1, 2018

Berk Aydın

ABBREVIATIONS AND SYMBOLS

ADS-B	Automatic dependent surveillance – broadcast
CA-CFAR	Cell Averaging – Constant False Alarm Rate
CUT	Cell Under Test
EKF	Extended Kalman filter
LSQ	Least Squares
MLE	Maximum Likelihood Estimation
PMR	Passive Multistatic Radar
RADAR	Radio Detection And Ranging
RSD	Radio Signal Data

f_{D}	Frequency of Doppler shift
$\boldsymbol{A}$	State transition matrix
$\boldsymbol{B}$	Control input model matrix
$\boldsymbol{H}$	Observation model matrix
$\boldsymbol{K}$	Optimal Kalman gain
$\boldsymbol{P}$	Error covariance matrix
$\boldsymbol{Q}$	Covariance of process noise
$\boldsymbol{R}$	Covariance of observation noise
$\mathbf{u}$	Control input vector
$\mathbf{v}$	Measurement noise vector
$\mathbf{w}$	Process noise vector
$\mathbf{x}$	State vector
$\mathbf{z}$	Observed state vector

List of Tables

1 Range of variables in lookup table 18

CONTENTS

1 INTRODUCTION **1**

1.1 Radar 1

1.2 Research Objectives 2

1.3 Organization of the Thesis 3

2 THEORY AND EXPERIMENTAL SETUP **4**

2.1 Experimental Setup 4

2.2 Mathematical Model 4

2.3 Signal Extraction 5

2.4 Kalman Filter 8

2.5 Extended Kalman Filter 10

2.6 Tracking 11

3 TRACK INITIALIZATION **12**

3.1 Identifying Doppler Curves 12

3.2 Optimization of Initial Parameters of EKF by Nearest Neighbor Search . 17

3.3 Maximum Likelihood Estimation 19

4 RESULTS **21**

4.1 Simulation Results 21

4.1.1 Nearest Neighbor Search 21

4.1.2 Maximum Likelihood Estimation 26

4.2 Experimental Results 28

5 DISCUSSION **30**

6 CONCLUSIONS **32**

6.1 Future Work 32

REFERENCES **33**

1 INTRODUCTION

1.1 Radar

Scottish physicist James Clerk Maxwell formulated the equations of the classical electromagnetic theory in the 19th century. He proposed that light is an electromagnetic phenomenon based on his famous work, Maxwell's equations. The theory also predicted an infinite number of frequencies of electromagnetic waves, which constitute the electromagnetic spectrum. Further theoretical works investigated how electromagnetic waves are reflected from surfaces and refracted by dielectric medium. German physicist Heinrich Hertz experimentally confirmed these properties using radio waves in the late 19th century. Hertz's work revealed the potential of detecting targets by radio waves.

In the beginning of 20th century Hülsmeyer experimented with the detection of radio waves reflected from ships. He obtained a patent for an obstacle detector and ship navigational device. His invention did not attract the attention of the German Navy, because its range was less than a mile and was not better than a visual observer. In 1922 A. H. Taylor and L. C. Young managed to detect a wooden ship using a bistatic continuous-wave radar with separated receiver and transmitter since the technology that allows an antenna to be switched from transmit to receive mode did not yet exist. L. A Hyland made the first detection of aircraft using wave-interference effect. The Naval Research Laboratory acquired the patent that was called as "System For Detecting Objects by Radio". The technology was refined and used extensively after the outbreak of the World War II. The further development of technology continued after the war and possible improvements such as measuring the Doppler shifts were investigated. [1]

Radar (**RA**dio **D**etection **A**nd **R**anging) is a surveillance system that detects position and velocity of objects by using low frequency electromagnetic waves, such as radio waves and microwaves. A classical setup of radio system consists of an illuminator that produces the electromagnetic waves and a receiver that detects the electromagnetic waves reflected from the target. A radar system whose transmitter and receiver are placed in close proximity is called a monostatic radar. A bistatic radar system uses transmitter and receiver antennas that are separated by a significant distance. Radar systems that contain multiple receivers that are scattered in a large area are called multistatic radar systems.

Bistatic or multistatic radars can work either with their own transmitters, which are only designed for the radar system, or with transmitters of opportunity, which are designed

for other purposes especially for broadcasting services. This is in contrast to monostatic radar, which uses a single antenna for both purposes.

In modern aviation, tracking of aircraft is supported by aircraft's onboard transmitters. Automatic dependent surveillance – broadcast (ADS-B) system determines the aircraft's position and velocity via GPS and broadcasts that information voluntarily [2]. Radar systems that do not depend on broadcasts from the target are called Non-Cooperative Systems. Objects that do not disclose their state information are called Non-Cooperative Target.

In this work, we focus on a Passive Multistatic Radar (PMR) system. Passive radar systems do not have their own transmitter. They depend on transmitters of opportunity to track objects independently from targets' own broadcast. Radio sources that emit analog TV signal and FM radio signal can be used as transmitters of opportunity. According to the work done in [3], the advantages and disadvantages of PMR are listed as below:

Advantages:

1. Receivers are undetectable.
2. They are lower cost, due to lack of transmitter.
3. Target position can be updated very fast.
4. Stealth aircraft can be detected.
5. They do not need any specific frequency allocations.

Disadvantages:

1. They have no control over the transmitter.
2. Their technology has not been fully developed yet.
3. Their geometry is more complex.

1.2 Research Objectives

The main focus of this study is to develop a track initialization algorithm as a supplement for the passive radar system that has been developed for several years [4] [5] [6] [7]

[8]. The goal of that project is developing an online multistatic passive radar system that relies only on the Doppler shifts that are caused by aircraft in the frequency of nearby radio signal sources. The radar system has the capability to track aircraft by the Extended Kalman filter (EKF) after the track has been initialized.

Track initialization algorithm has two objectives. First, the Doppler shifts in the radio signal data (RSD) have to be extracted without using any other radio or information source such as ADS-B. This allows us to determine the initial points of detections and follow the curves in the observed RSD. The second objective is to determine the state of aircraft at the initial point. Therefore, EKF can be initialized by a good estimate of the state and thereafter provide accurate estimates. Possible improvements over the initial estimate are also investigated.

1.3 Organization of the Thesis

The organization of this thesis is as follows. Section 2 introduces the mathematical model and the experimental setup. We describe the physics behind the Doppler shift and tools to extract the data. The last sections of Section 2 is focusing on reviewing The Kalman Filter.

Section 3 provides a detailed description of the algorithms we developed for tracking initialization. We conduct both analytical and simulation studies to investigate the performance of the algorithms and show the results in Section 4.

In Section 5, we briefly discuss the results. Section 6 gives a summary of this dissertation and possible directions for future work.

2 THEORY AND EXPERIMENTAL SETUP

2.1 Experimental Setup

Our experimental setup consists of 7 receivers located in Eastern Finland. Antennas are connected to Raspberry Pi computers and operate asynchronously. The radio source is the 326 meters tall Saint Petersburg TV Tower. For this experiment, the receivers have been configured in order to acquire signals within 100 Hz range of the transmitted frequency with 1 Hz precision. Figure 1 shows the setup.

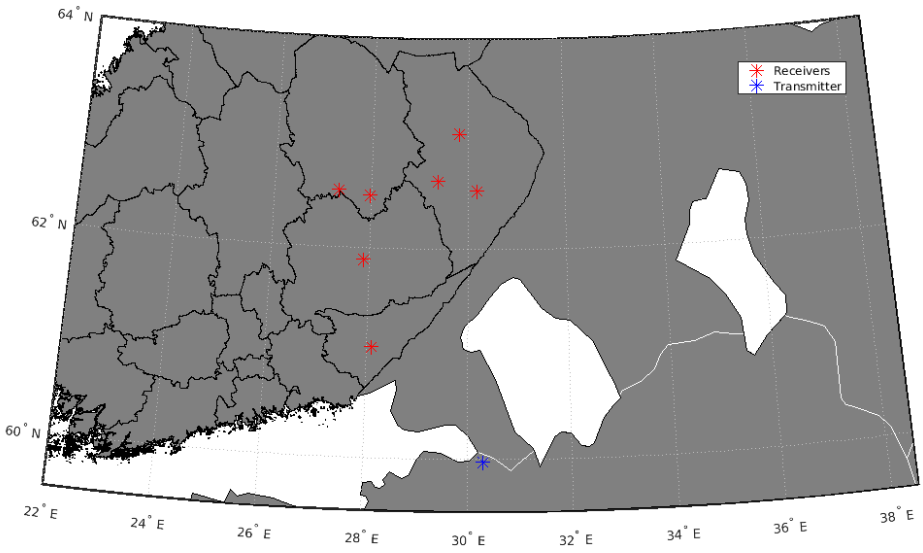

Figure 1. Positions of receivers (red) and transmitter (blue)

2.2 Mathematical Model

The Doppler shift is the change in the frequency of a wave due to the relative motion of the observer with respect to the source [9]. In our setup, the radio transmitter and the receivers are stationary. The Doppler shift is observed in the reflected waves coming

from the aircraft. The equation that describes the observed frequency change is defined in Eq. 1.

$$f_{\mathrm{D}}(t) = \frac{f_0}{c} \frac{\mathrm{d}(d_{\mathrm{AT}}(t) + d_{\mathrm{AR}}(t))}{\mathrm{d}t} \tag{1}$$

where $f_{\mathrm{D}}(t)$ is the observed Doppler shift at time t, f_0 is the frequency of the emitted wave, c is the speed of light, $d_{\mathrm{AT}}(t)$ is the distance between the aircraft (A) and the transmitter (T) at time t and $d_{\mathrm{AR}}(t)$ is the distance between the aircraft and the receiver (R) at time t. The distances $d_{\mathrm{AT}}(t)$ and $d_{\mathrm{AR}}(t)$ are great circle distances and calculated according to Eq. 2.

$$d_{\mathrm{AT}}(t) = \sqrt{2R_{\mathrm{e}}(R_{\mathrm{e}} + h(t))(1 - cos(\alpha_{\mathrm{AT}}(t))) + h(t)^2} \tag{2}$$

where R_{e} is the mean radius of the Earth, $h(t)$ is the altitude of the aircraft at time t, $\alpha_{\mathrm{AT}}(t)$ is the great circle arc between the aircraft and the transmitter at time t and it is measured in radians. $d_{\mathrm{AR}}(t)$ is calculated in the same manner. Figure 2 illustrates the geometry of the model and how the angles are defined.

2.3 Signal Extraction

The RSD consists of time series data that have been recorded in several locations. The signal is transformed into time-frequency domain by Fourier Transform (Figure 4.a). The x-axis is centered around the frequency of the transmitter (baseline) and extended by 100 Hz to both positive and negative directions. The y-axis represents the time. The curves that intersects the baseline are Doppler shifts caused by the aircraft.

The statistically significant features of the data must be extracted in order to analyze the data. We are using Cell Averaging – Constant False Alarm Rate (CA-CFAR) method as explained in [10]. Each pixel in the image (Figure 4.a) is treated as a cell. The cell under test (CUT) is compared to the reference cells (Figure 3). Reference cells determine the background level of the signal and guard cells form a barrier between CUT and reference cells so that signal amplitude in those are independent from each other. The comparison is done according to Eq.3:

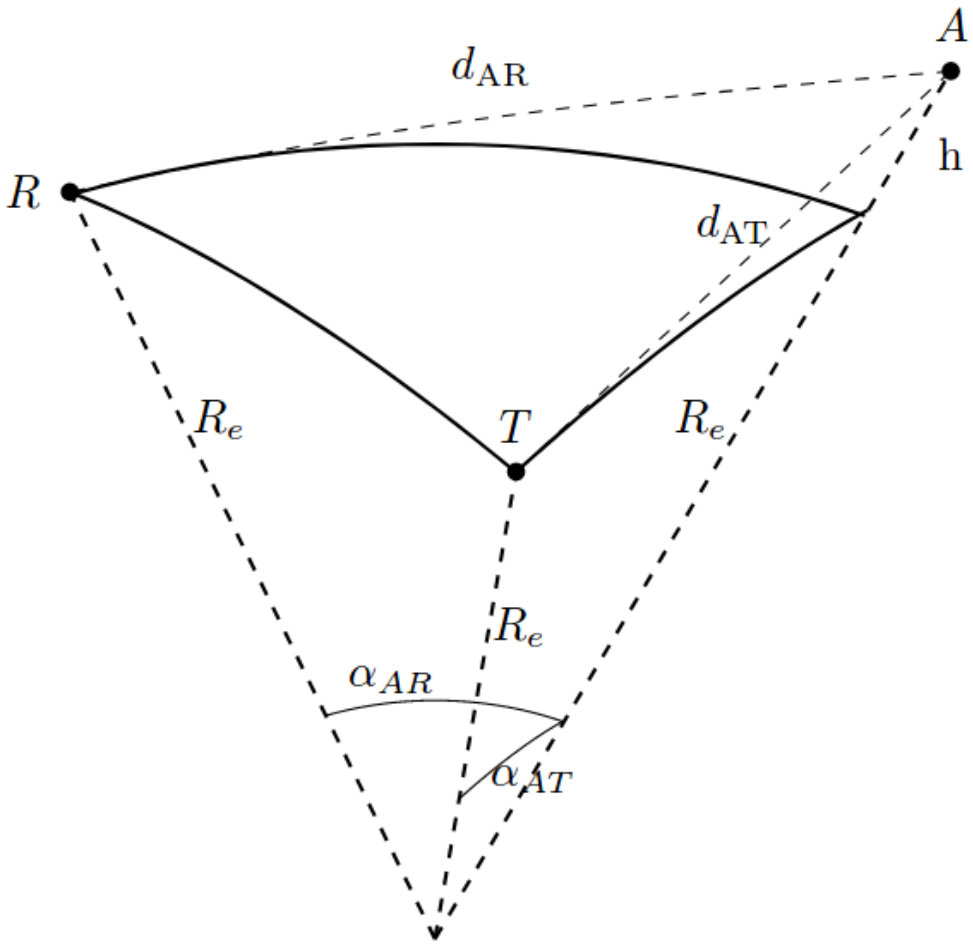

Figure 2. Geometry of the model

$$C_{\mathrm{CUT}} > N(P_{fa}^{-\frac{1}{N}} - 1)\frac{1}{N}\sum_{i=1}^{N} C_{\mathrm{ref}}(i) \tag{3}$$

where N is the number of reference cells, P_{fa} is the desired false alarm rate, C_{CUT} and C_{ref} are signal amplitude of the cell under test and reference cells. The cells that satisfy the inequality are stored in the extracted data (Figure 4.b). The extracted data is binary; for a given time and frequency the cell contains a signal or not. It has no information regarding the signal amplitude as it is irrelevant for tracking purposes.

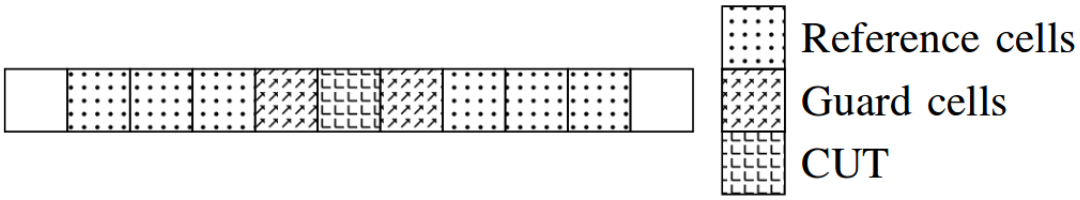

Figure 3. Arrangement of cells for CA-CFAR

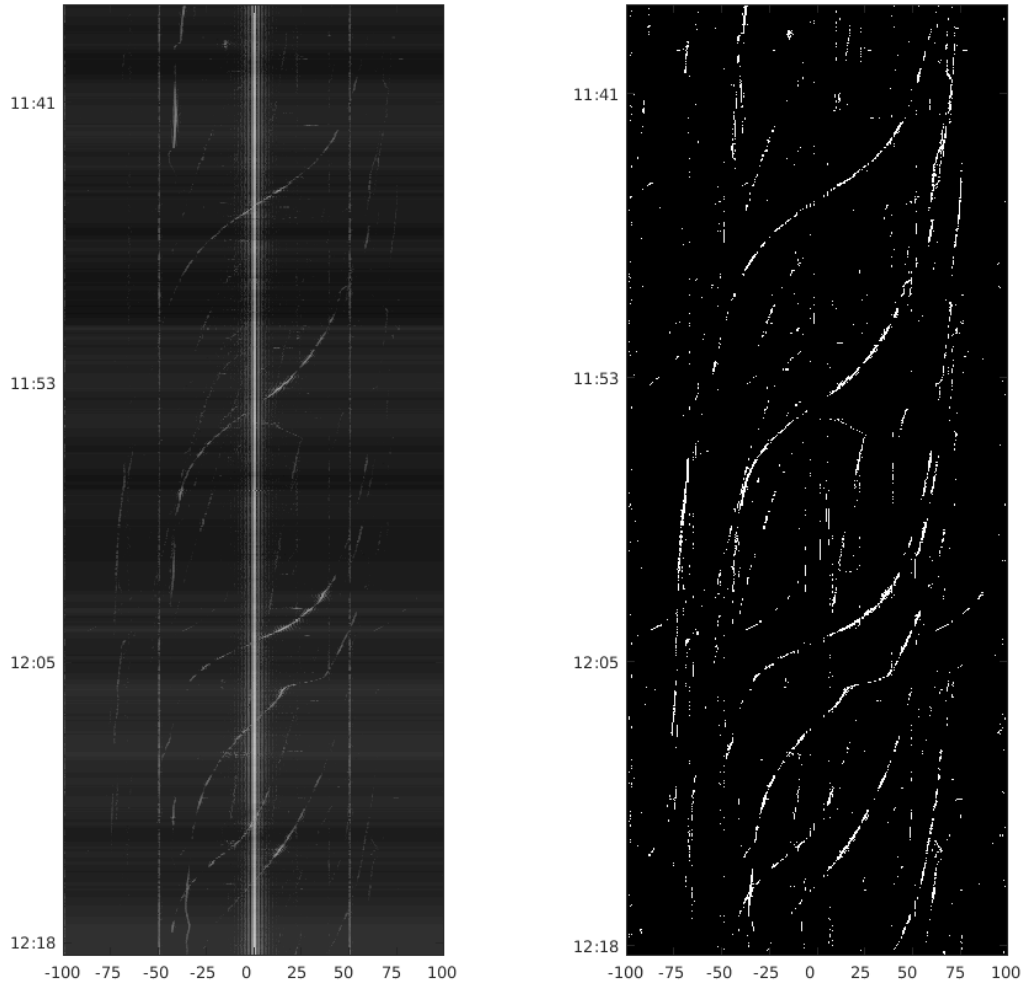

(a) Raw data

(b) Extracted data with CA-CFAR (Baseline is removed.)

Figure 4. Signal extraction

2.4 Kalman Filter

The Kalman filter is a predictor-corrector type estimator which works by keeping the estimated error covariance to a minimum in linear systems. The Kalman filter is widely used in mathematical models about guidance, navigation, and control of vehicles. It consists of a few mathematical equations which describe two steps which work together as a form of feedback control [11]. Figure 5 illustrates the process.

The first part of developing a linear Kalman filter involves describing the linear stochastic difference Eq. 4 which is relevant to the discrete-time RSD studied in this work. From this equation the state, $\mathbf{x}_k \in \Re^n$, can be estimated with a measurement, $\mathbf{z}_k \in \Re^m$, as shown in Eq. 5. The matrix $\mathbf{A}_k$ $(n \times n)$ represented in Eq. 4 is the state transition matrix at kth timestep and relates the state of the model at previous timestep $k-1$ to the current time step k. $\mathbf{B}_k$, from Eq. 4, is an $n \times l$ matrix which relates the state $\mathbf{x}$ to the optional control input $\mathbf{u}_k \in \Re^l$, which is zero in our case as passive radar observations have no impact or control on the flight trajectory. $\mathbf{H}_k$, from Eq. 5, is the $m \times n$ observation model matrix which relates the current state of Eq. 4 to the measurement $\mathbf{z}_k$.

$$\mathbf{x}_k = \mathbf{A}_k\mathbf{x}_{k-1} + \mathbf{B}_k\mathbf{u}_k + \mathbf{w}_k \tag{4}$$

$$\mathbf{z}_k = \mathbf{H}_k\mathbf{x}_k + \mathbf{v}_k \tag{5}$$

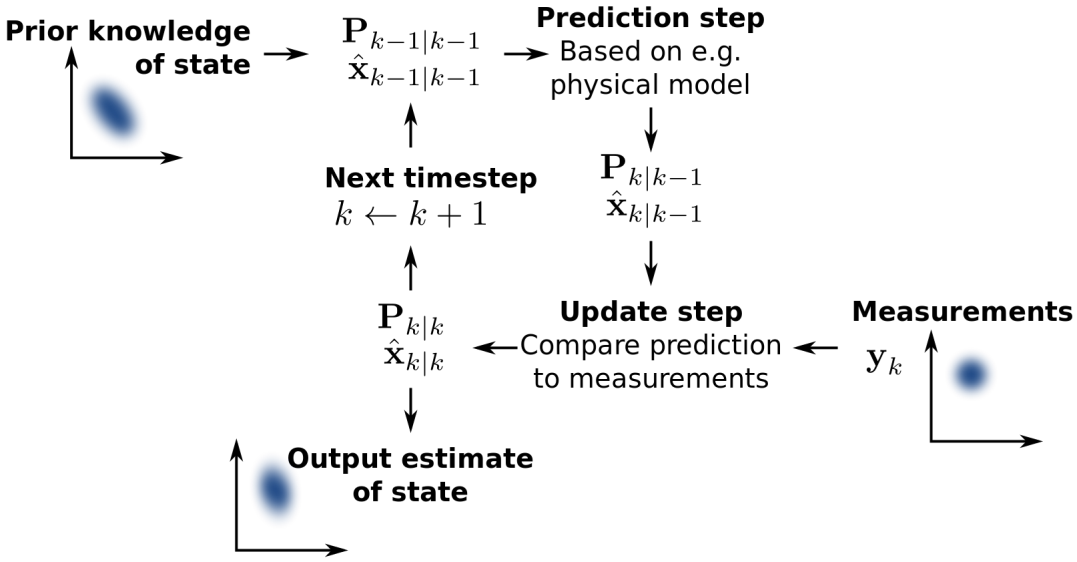

Figure 5. Basic concept of Kalman filtering [12]

The variables $\mathbf{w}_k$ and $\mathbf{v}_k$ are both random variables and they are representative of the fact that both the process and the measurements contain noise. They are both independent of each other and are assumed to be normally distributed. They are represented by the probability distributions in Eq.6 and Eq.7. $\mathbf{Q}$ and $\mathbf{R}$ are matrices that represent the process noise covariance and the measurement noise covariance respectively.

$$p(w) \sim N(0, \mathbf{Q}) \tag{6}$$

$$p(v) \sim N(0, \mathbf{R}) \tag{7}$$

The second part of producing a Kalman filter involves making two sets of equations. These two sets are the time update equations and the measurement update equations.

The following set of equations are the time update equations and they represent the prediction part of the Kalman filter. These equations are responsible for projecting the current state and error covariance in order to obtain an *a priori* estimate for the next time step. These equations are represented in Eq.8 and Eq.9:

$$\hat{\mathbf{x}}_{k|k-1} = \mathbf{A}\hat{\mathbf{x}}_{k-1|k-1} + \mathbf{B}_k\mathbf{u}_k \tag{8}$$

$$\mathbf{P}_{k|k-1} = \mathbf{A}_k\mathbf{P}_{k-1|k-1}\mathbf{A}_k^{\mathrm{T}} + \mathbf{Q}_k \tag{9}$$

where $\hat{\mathbf{x}}_{k|k-1}$ is the *a priori* state estimate at kth timestep given observations up to timestep $k-1$ and $\mathbf{P}_{k|k-1}$ is the *a priori* error covariance matrix at kth timestep.

The second set of equations are known as the measurement update equations and represent the correction part of the estimator. The equations are shown in Eq.10, Eq.11 and Eq.12:

$$\mathbf{K}_k = \mathbf{P}_{k|k-1}{\mathbf{H}_k}^{\mathrm{T}}(\mathbf{H}\mathbf{P}_{k|k-1}{\mathbf{H}_k}^{\mathrm{T}} + \mathbf{R})^{-1} \tag{10}$$

$$\hat{\mathbf{x}}_{k|k} = \hat{\mathbf{x}}_{k|k-1} + \mathbf{K}_k(\mathbf{z}_k - \mathbf{H}_k\hat{\mathbf{x}}_{k|k-1}) \tag{11}$$

$$\mathbf{P}_{k|k} = (\mathbf{I} - \mathbf{K}_k\mathbf{H}_k)\mathbf{P}_{k|k-1} \tag{12}$$

where $\mathbf{K}_k$ is the optimal Kalman gain at time k, $\hat{\mathbf{x}}_{k|k}$ is the *posteriori* state estimate at kth timestep given observations up to kth timestep and $\mathbf{P}_{k|k}$ is the *posteriori* error covariance matrix at kth timestep.

2.5 Extended Kalman Filter

The extended Kalman filter is the nonlinear version of the Kalman filter. Due to the nonlinear nature of the system we are analyzing, we used EKF in our work to track the motion of the aircraft.

EKF relies on the differentiability of the state transition and observation functions, rather than their linearity. The state distribution is propagated analytically through the first-order Taylor series expansion of the nonlinear system.

Formulation of the EKF can be done as follows with the same notation used in the Section 2.4 according to [13]:

$$\mathbf{x}_k = f(\mathbf{x}_{k-1}, \mathbf{u}_k) + \mathbf{w}_k \tag{13}$$

$$\mathbf{z}_k = h(\mathbf{x}_k) + \mathbf{v}_k \tag{14}$$

where f is the state transition function that computes the predicted state from the previous estimate and h is the observation function that predicts measurement from the predicted state.

Prediction step of the EKF is done as follows:

$$\hat{\mathbf{x}}_{k|k-1} = f(\mathbf{x}_{k-1|k-1}, \mathbf{u}_k) \tag{15}$$

$$\mathbf{P}_{k|k-1} = \mathbf{A}_k \mathbf{P}_{k-1|k-1} \mathbf{A}_k^{\mathrm{T}} + \mathbf{Q}_k \tag{16}$$

where $\mathbf{A}_k$ is the state transition matrix at kth timestep obtained by the following Jacobian:

$$\mathbf{A}_k = \frac{\partial f}{\partial \mathbf{x}}\Big|_{\hat{\mathbf{x}}_{k-1|k-1}, \mathbf{u}_k} \tag{17}$$

After the prediction step, state estimate and estimate covariance are updated.

$$\mathbf{K}_k = \mathbf{P}_{k|k-1} \mathbf{H}_k{}^{\mathrm{T}} (\mathbf{H} \mathbf{P}_{k|k-1} \mathbf{H}_k{}^{\mathrm{T}} + \mathbf{R})^{-1} \tag{18}$$

$$\hat{\mathbf{x}}_{k|k} = \hat{\mathbf{x}}_{k|k-1} + \mathbf{K}_k (\mathbf{z}_k - \mathbf{H}_k \hat{\mathbf{x}}_{k|k-1}) \tag{19}$$

$$\mathbf{P}_{k|k} = (\mathbf{I} - \mathbf{K}_k \mathbf{H}_k) \mathbf{P}_{k|k-1} \tag{20}$$

where $\mathbf{H}_k$ is the observation matrix at kth timestep obtained by the following Jacobian:

$$\mathbf{H}_k = \frac{\partial h}{\partial \mathbf{x}}\Big|_{\hat{\mathbf{x}}_{k|k-1}} \tag{21}$$

2.6 Tracking

Tracking of aircraft is an inverse problem in which the state of the aircraft is determined by the observed Doppler shift it causes. Extracted Doppler curves are used to feed the EKF to track the aircraft. The state vector $\mathbf{x}_k$ is defined as:

$$\mathbf{x}_k = [\phi_k \quad \lambda_k \quad \dot{\phi}_k \quad \dot{\lambda}_k \quad l_k]^{\mathrm{T}} \tag{22}$$

where ϕ_k is the latitude of the aircraft, λ_k is the longitude of the aircraft, $\dot{\phi}_k$ and $\dot{\lambda}_k$ are time derivatives of latitude and longitude, respectively and l_k is the altitude of the aircraft at kth timestep. Predicted Doppler shift for each receiver can be calculated from the state vector using Eq. 1. Since Eq. 1 is a nonlinear function, its Jacobian is used as an observation matrix in EKF. The ith row of the Jacobian that corresponds to ith receiver at kth timestep can be written as:

$$\mathbf{H}_k^i = \frac{\partial f_{\mathrm{D}}^i(\mathbf{x})}{\partial \mathbf{x}}\Big|_{\hat{\mathbf{x}}_{k|k-1}} \tag{23}$$

$$= [\frac{\partial f_{\mathrm{D}}^i(\mathbf{x})}{\partial \phi_k} \quad \frac{\partial f_{\mathrm{D}}^i(\mathbf{x})}{\partial \lambda_k} \quad \frac{\partial f_{\mathrm{D}}^i(\mathbf{x})}{\partial \dot{\phi}_k} \quad \frac{\partial f_{\mathrm{D}}^i(\mathbf{x})}{\partial \dot{\lambda}_k} \quad \frac{\partial f_{\mathrm{D}}^i(\mathbf{x})}{\partial l_k}] \tag{24}$$

The state transition matrix that is applied to the state vector is a linear function and it can be used without any further transformation. It is defined as:

$$\mathbf{A} = \begin{bmatrix} 1 & 0 & \Delta t & 0 & 0 \\ 0 & 1 & 0 & \Delta t & 0 \\ 0 & 0 & 1 & 0 & 0 \\ 0 & 0 & 0 & 1 & 0 \\ 0 & 0 & 0 & 0 & 1 \end{bmatrix} \tag{25}$$

The tracking process is carried out as it is explained in Section 2.5. The missing measurements due to observational gaps or aircraft not being in the range of a receiver are skipped during the state is updated (Eq. 19). Intrinsic uncertainty of EKF at timestep k can be calculated from its covariance matrix $\mathbf{P}_{k|k}$ and the tracking process is finalized when the uncertainty exceeds the predetermined uncertainty limit.

3 TRACK INITIALIZATION

In order to track the motion of an aircraft, we use the setup explained in Section 2.1, process the signal using the methods mentioned in Section 2.3 and estimate the flight path of the aircraft using EKF as discussed in Section 2.5. One of the vital points of the whole process is determining when and how to initialize EKF with proper initial parameters. The radar system we are working on must be independent of human interference and be able to decide when to initialize and finalize the tracking without using any other sources such as ADS-B. In this section, we focus on the track initialization algorithm, which works real-time and autonomously.

RSD is collected in a way that there is an approximately 3 second interval between each time step and 1 Hertz resolution in the frequency domain. Our main transmitter of interest is the Saint Petersburg TV Tower. We record in the frequency range of +/- 100 Hz around the broadcasting frequency of the Saint Petersburg TV Tower.

3.1 Identifying Doppler Curves

The signal in RSD comes from 3 different sources: The transmitter itself, reflected waves from aircraft and random noise. Our first goal is identifying the Doppler curves in RSD (Figure 4.a) that are caused by aircraft so that EKF can run on them.

RSD is extracted as discussed in Section 2.3. After the extraction, the constant frequency that transmitter broadcasts (baseline) at is removed (Figure 4.a). The rest is Doppler curves from aircraft and noise.

The objective of this part is separating Doppler curves from noise also following their path in time in order to distinguish curves from different sources while merging the ones from the same source. As it can be seen from Figure 4.a and Figure 8.a, observational gaps within the same Doppler curve from the same aircraft can occur. The algorithm we developed merges curves if it concludes that they are from the same aircraft.

We expect to detect aircraft that are moving towards the receivers (but not necessarily with a perpendicular angle), so the algorithm assumes that the Doppler shift starts with an initial observation in the positive side of the time-frequency domain as the objects moving towards the observer cause an increase in the frequency. The algorithm starts with

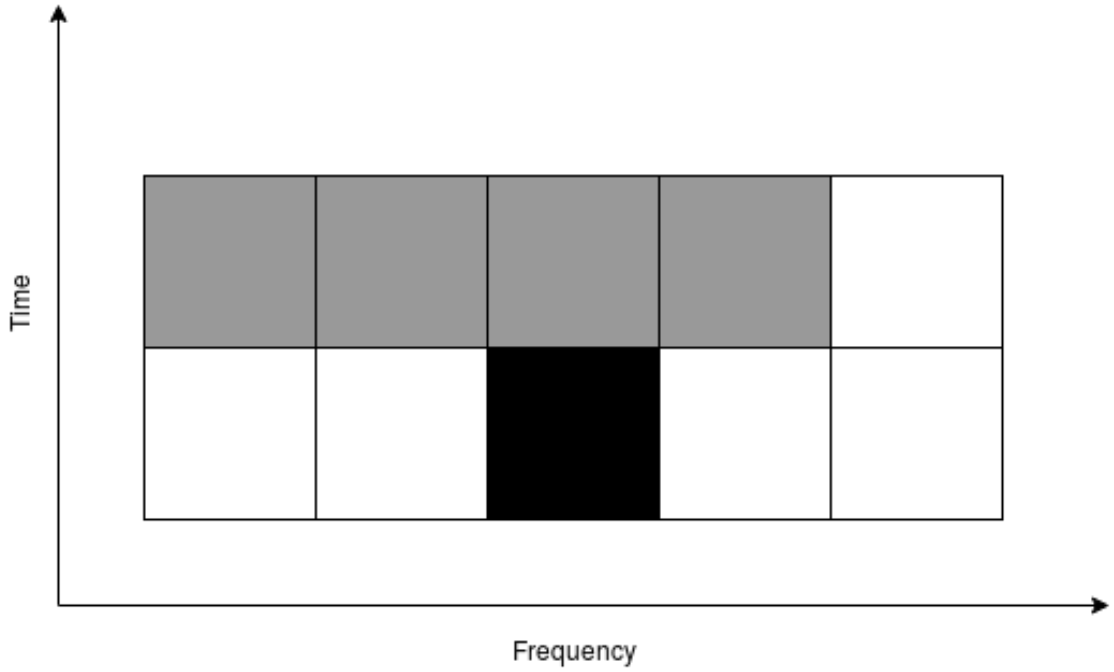

Figure 6. Arrangement of candidate cells (grey) that follow the detected cell (black)

the first data extracted by CA-CFAR. It works in an online way such that each timestep is processed in order. Cells that are in the next time step and in the close proximity to the detected cell in the current time step are considered as candidate cells (Figure 6). Arrangement of candidate cells are chosen to be left-skewed due to the nature of our setup. Doppler shift of an incoming aircraft is expected to be decreasing or constant with time. The algorithm follows the curves through candidate cells and if one of the candidate cells are also marked as detected by CA-CFAR, we have a consecutive detection. After reaching an arbitrary number of consecutive detections (n_{det}) algorithm marks the initial point as a starting point of a Doppler curve that is generated by an aircraft and tracking is initialized (Blue asterisks in Figure 8.b). A higher choice of n_{det} would provide a lesser false positive rate but also delay the start of tracking.

The algorithm continues to follow the curves after the initialization until they cross the baseline. By doing so it prevents initialization of the same flight in the future. Following the identified curves has two major challenges:

1. Following the curve through the observational gaps.
2. Following multiple Doppler curves from different aircraft that intersect. While intersection of curves is an extremely rare event in the Finnish skies, observational gaps occur frequently.

We tried to solve the first challenge as described below and left the second challenge for future work.

Observational gaps are classified into two categories according to their duration and different solutions are developed for each category. The observational gaps that last less than 4 timesteps (approximately 13 seconds) are classified as short gaps. The gaps whose duration are between 5 and 20 timesteps are classified as long gaps. Any gap that lasts more than 20 timesteps are excluded from this investigation, since they cannot be followed accurately.

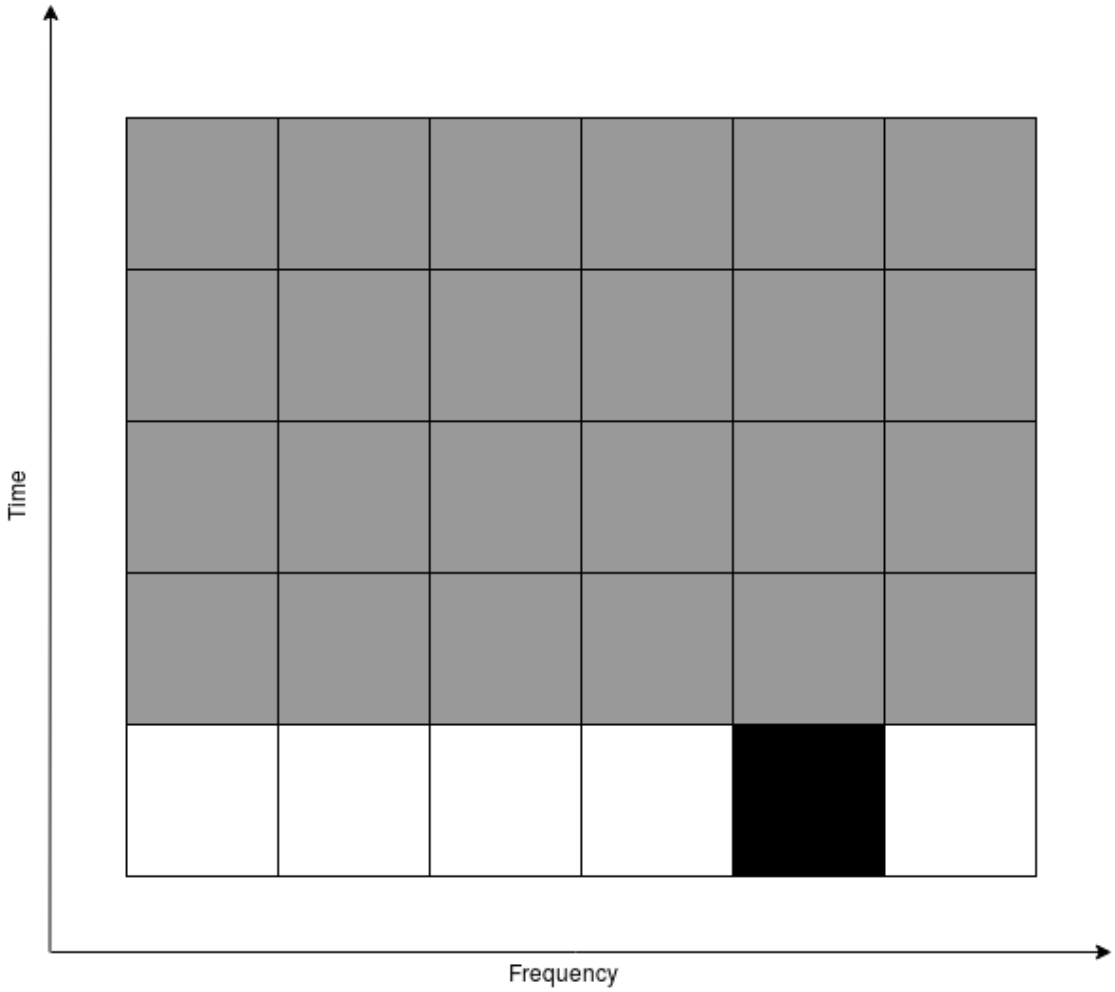

Figure 7. Arrangement of extended candidate cells (grey) that follow the detected cell (black) for already identified curve

The algorithm firstly checks for small gaps if there is no detection among candidate cells in an identified track. We saw that following through the short gaps can be done by simply extending the reach of candidate cells (Figure 7). Arrangement of extended candidate cells are also chosen to be left-skewed. Any detected cell among the extended candidate

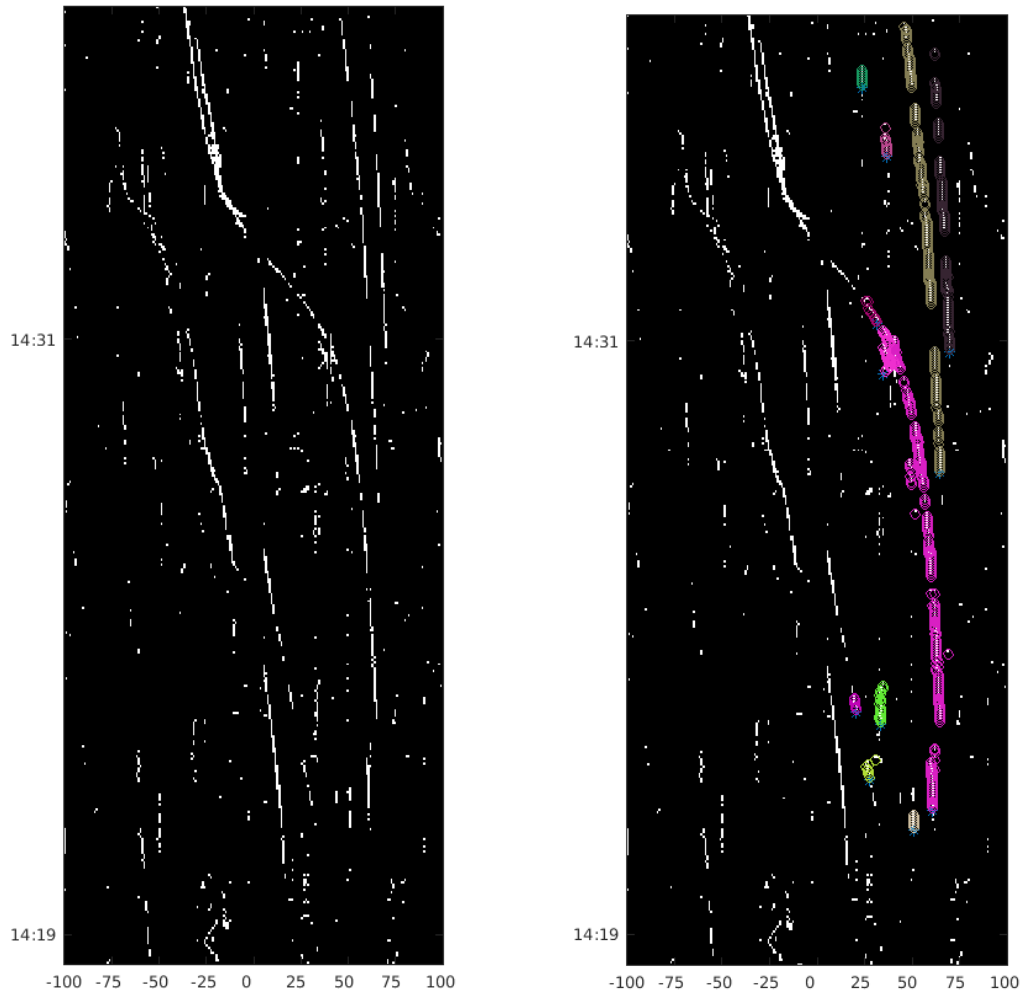

(a) After CA-CFAR (baseline is removed)

(b) Identified Curves. Curves marked with different color represent different flights

Figure 8. Identified Doppler Curves

cells is added to the identified track and the algorithm continues to follow. In case of no detection among extended candidate cells, the algorithm proceeds to check for long gaps.

Simply extending candidate cells more cannot be used in search for long gaps. The area they cover would be too broad and could include detected cells that are irrelevant to the Doppler curve that is followed. We can avoid this problem by predicting where the cells would be if there had been no gap. We achieved this by extrapolating the curve for 20 timesteps using a second degree polynomial. The polynomial fit is done in the least squares (LSQ) sense using all the points in the track. Cells that are in close proximity of the extrapolated curve are considered as canditate cells and the earliest candidate cell that is detected is added to the identified track. The search continues until no suitable cells are found in the long gap search.

Tracking can start immediately after a starting point (Blue asterisks in Figure 8.b) is detected in one receiver. However, we saw that having at least four receivers significantly improves the estimate of EKF and the choice of initial of parameters. We decided to initialize the tracking when at least four receivers identify a starting point. Multi-object tracking is not in the scope of this study. It is assumed that no more than one unidentified aircraft is in the range of receivers at the same time.

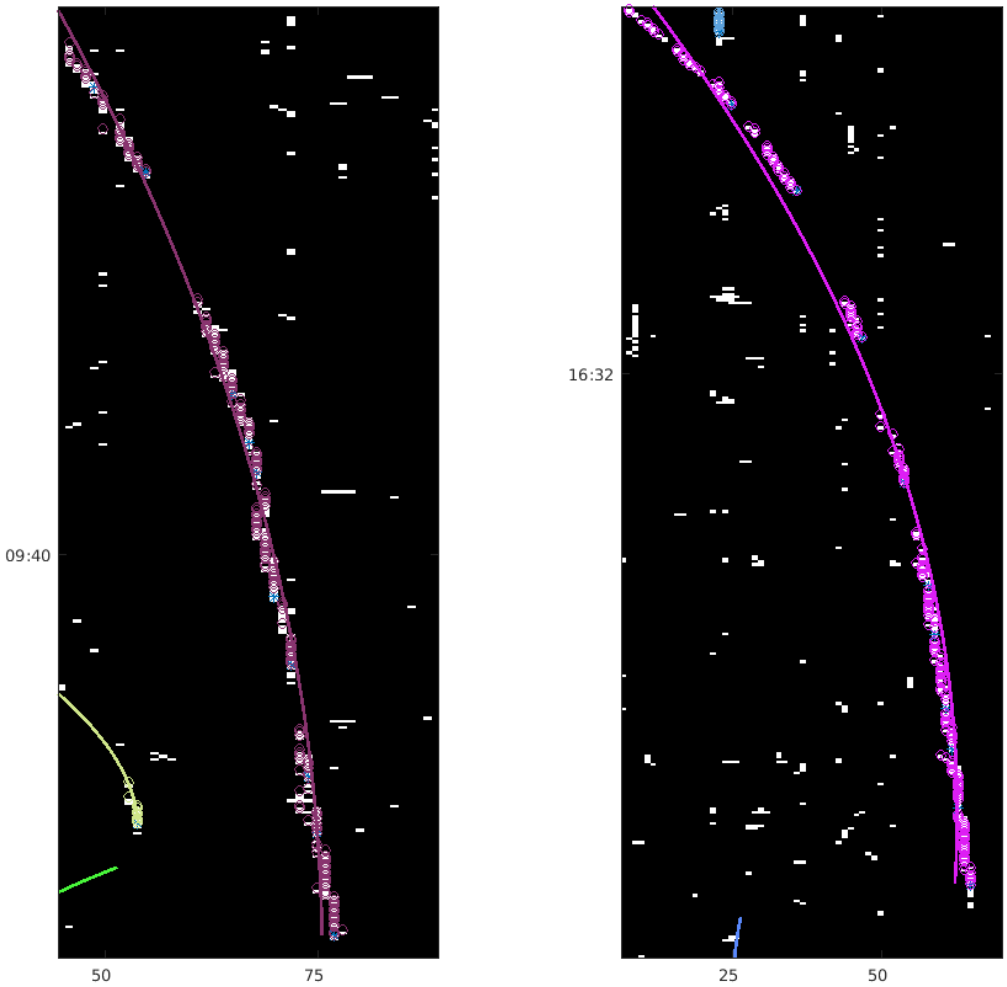

(a) (b)

Figure 9. Fitted Polynomials (continuous lines)

3.2 Optimization of Initial Parameters of EKF by Nearest Neighbor Search

In Section 3.1 we investigated when to initialize the Extended Kalman Filter (EKF). In this section we investigate how to initialize the EKF. The EKF might not converge quickly, or worse, diverge if it is not initialized properly with an appropriate choice of initial parameters [14].

The observed magnitude of the Doppler shift caused by an aircraft depends on five variables (latitude, longitude, bearing, speed and altitude of the aircraft) and four constants (positions of receiver and transmitter antennas). The problem of calculating the initial state of the aircraft only via Doppler shift measurements from several receivers is impossible to solve analytically.

We investigated the means of estimating the initial state using a model based on a nearest neighbor search algorithm. The scope of this work is limited to commercial planes which fly on designated air routes. Characteristics of air routes do not change drastically with time. We developed a lookup table based on historical data of previous flights and artifically created flights simulated by a model to represent the characteristic of air routes in the range of our receivers. The data point in the lookup table with the most similar characteristics (nearest neighbor) to the observed data is chosen to be the initial state.

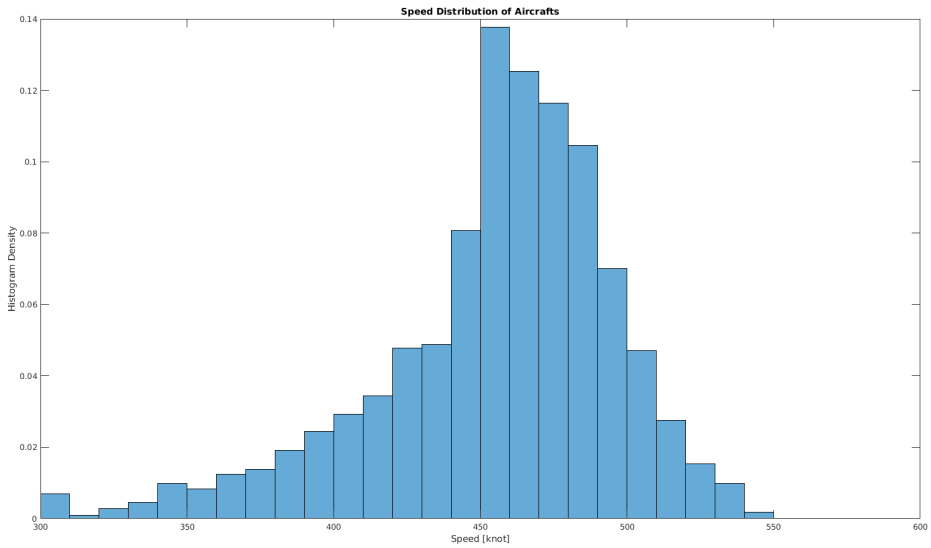

Figure 10. Distribution of cruise speed of aircraft at the time of initialization

Table 1. Range of variables in lookup table

Variable	Values	Unit
Latitude	24:0.05:34	Degree
Longitude	60:0.05:64	Degree
Bearing	0:1:359	Degree
Altitude	35000	Foot
Speed	430,460,490	Knot

The lookup table was generated in such a way to cover the desired range of all variables (latitude, longitude, bearing, speed and altitude of the aircraft) and their corresponding predicted Doppler shift for each receiver. The interval of longitutude and latitude was determined with respect to the range of the receivers. The range of bearings are chosen to cover all possible angles. After a thorough analysis, we concluded that the effect of altitude on measured Doppler shifts is less than the precision of measurement and it can be neglected, so a single value of altitude is chosen for faster search performance. Historical data was studied with the help of ADS-B in order to determine the cruise speeds at the time of initialization. According to the distribution of cruise speed of aircraft at the time of initialization (Figure 10), a suitable set of speeds were chosen. Table 1 displays the range of variables.

The lookup table also contains state information of several hundred flights from historical data. They were collected via aircraft's ADS-B broadcast. We aim to achieve a more accurate representation of flight characteristics by combining artificially created data points and historical data points. The lookup table reached to more than 17 million rows of data, each representing either a different combination of variables or historical data. We decided to reduce the number of rows to improve the performance of the searching process with the following assumptions:

At the time of initialization,

1. The aircraft is moving towards the receivers.
2. The aircraft is not very close to receivers.

We removed the rows that represent flights that are moving away from the receivers or located between the receivers, from the lookup table. These rows cannot serve as an initialization point as any flight with these characteristics should have already been initialized or cannot be initialized since they are already distant and moving away. After

removing rows according to these two assumptions, the number of rows is reduced to 7 million.

Each row in the lookup table includes the predicted Doppler shift values for each receiver, calculated using Eq. 1 according to the state parameters in that row. The observed Doppler shifts of an initial point, which is detected by the algorithm mentioned in Section 3.1, are compared to the predicted values in the lookup table. The distance between points is measured in Euclidean distance (l^2-norm). The distance between the ith row with n Doppler shifts $f_1^i, f_2^i, ..., f_n^i$ and the initial point with Doppler shifts $f_1^0, f_2^0, ..., f_n^0$ is calculated as:

$$d = \sum_{j=1}^{n} (f_j^i - f_j^0)^2 \tag{26}$$

The row that satisfied the minimum distance is chosen as the nearest neighbor. The parameters of the nearest neighbor is used as initial parameters in EKF and tracking continues with EKF until the aircraft is out of range or error of the prediction exceeds the predetermined limit.

3.3 Maximum Likelihood Estimation

We further investigated the means of improving the choice of initial parameters. One method we tried is Maximum Likelihood Estimation (MLE). It is an estimation method of parameters of a statistical model, given the observations. MLE is based on the likelihood function, which is a function of the parameters of a statistical model. It describes the plausability of the parameters of the model, according to the observations. MLE attempts to find the parameters that give the maximum likelihood if a maximum exists, given the observations. MLE is defined as:

$$\hat{\theta} \in \{\arg\max_{\theta \in \mathbf{\Theta}} \mathcal{L}(\theta; \mathbf{x})\} \tag{27}$$

where $\hat{\theta}$ is the estimator of the parameters, $\mathcal{L}$ is the likelihood function, θ is the vector of parameters of the model, $\mathbf{\Theta}$ represents the parameter space and $\mathbf{x}$ is the observed outcome.

We assumed that errors in parameters are distributed in the parameter space according to a multivariate Gaussian distribution with an arbitrarily chosen variance (Eq. 28).

$$\mathcal{L}(\theta; \mathbf{x}) = \frac{1}{\sigma\sqrt{2\pi}} e^{-(f_{\mathrm{D}}(\theta) - \mathbf{x})^2 / 2\sigma^2} \tag{28}$$

The parameter values that provide the minimum error satisfies the maximum likelihood condition. The minimum error search is done by MATLAB's `fminsearch` function, which is based on the Nelder–Mead simplex algorithm. The Nelder–Mead method attempts to minimize a nonlinear function without any implicit or explicit derivative information [15]. The initial parameters from the lookup table are inputted to `fminsearch` as an initial guess and the parameters that provide the minimum error are sought. Improvement over initial parameters by MLE is discussed in Section 4.1.2.

4 RESULTS

The purpose of these tests is to measure the performance of our algorithms and the experimental setup. The tests were made in two stages: simulation and experimental. In the simulation part, we have full control of the design of the experiment and we are able to analyze every aspect of the algorithm free of any constraints. In the experimental part, we analyzed how our system performed with the real data.

4.1 Simulation Results

We have investigated the error in initial parameters of aircraft determined by nearest neighbor search and possible improvements by maximum likelihood estimation.

4.1.1 Nearest Neighbor Search

Simulation we used is based on a Monte Carlo method. A large number of simulated data was generated and some statistical procedures were performed. Candidate initial points for tracking purposes were generated randomly with the following rules that were applied to variables: Latitude and longitude are uniform random variables between 24 and 34 degrees and 60 and 64 degrees, respectively. Bearing of the aircraft can be any direction. Speed of the aircraft is also a uniformly random between 420 and 500 knot. We have already decided that the altitude has neglicible effect on observed Doppler shifts and it was chosen as a single value. We have assumed that tracking would already be initialized for aircraft that are inside area surrounded by receivers. Those points were omitted from the simulation.

The simulation was done in four stages in order to study the effects of different observational setups. Tracking can be initiliazed with fewer receivers or it is possible to wait until the aircraft is detected by all receivers. The former provides an earlier initialization time and the latter provides a more precise choice of initial parameters. This trade-off is studied with tracks initialized with 4 and 7 receivers. Another point of interest is the resolution of the observations. We investigated two cases with 1 Hz resolution and 0.125 Hz resolution.

10,000 data points were genetared randomly for each case. Figures 11, 12, 13 and 14

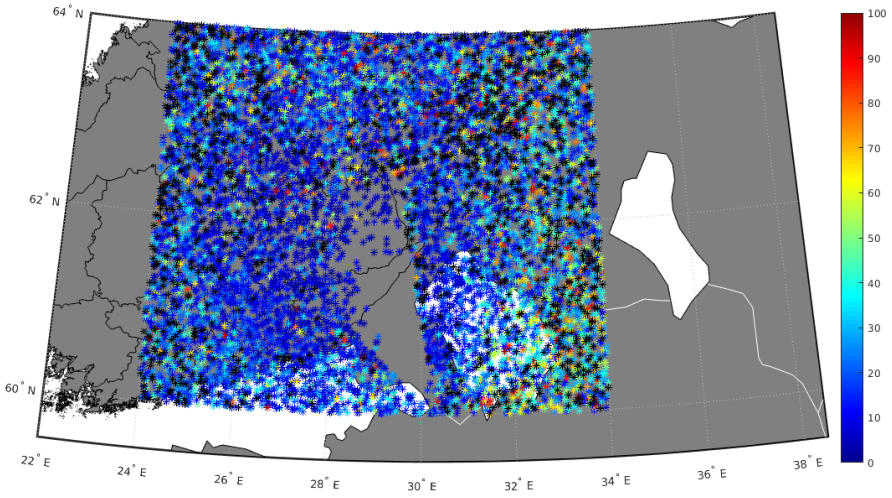

Figure 11. Error distribution with 1 Hz resolution and 4 receivers

represent the errors in distance for the shown position. Errors in km are represented by their color as explained by the colorbar on the right side of the graph. Errors more than 100 km are represented by black points.

Errors distributions in distance, speed and bearing are also investigated for each case. Figures 15, 16 and 17 illustrate the corresponding distributions, in logaritmic scale.

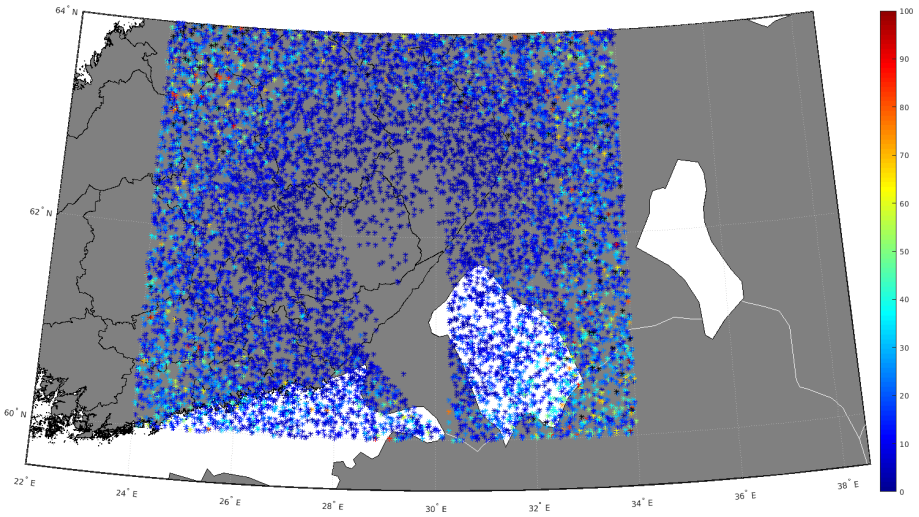

Figure 12. Error distribution with 1 Hz resolution and 7 receivers

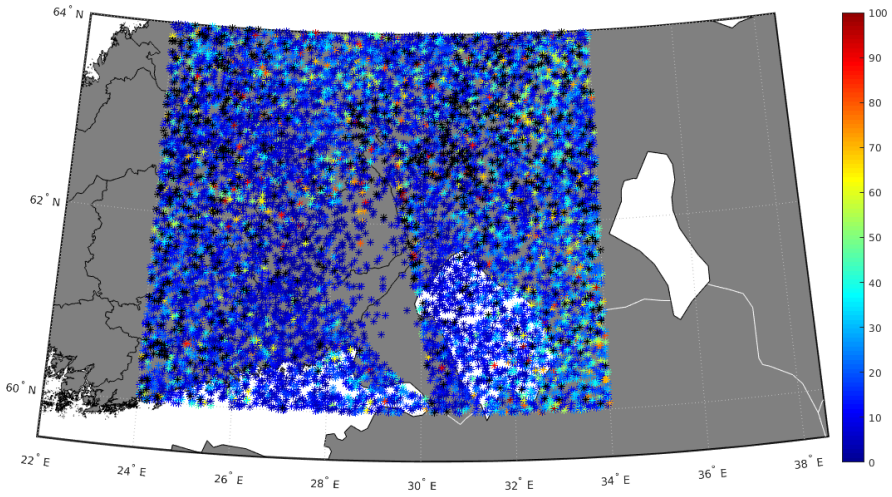

Figure 13. Error distribution with 0.125 Hz resolution and 4 receivers

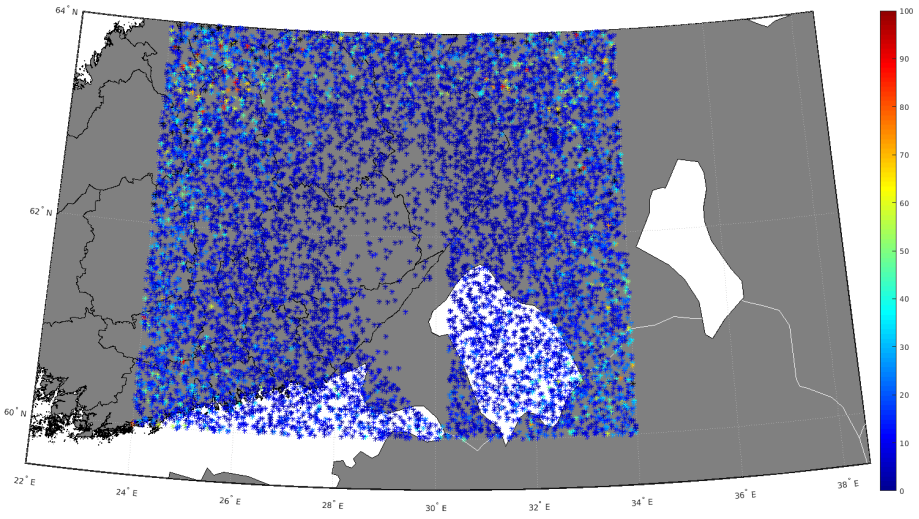

Figure 14. Error distribution with 0.125 Hz resolution and 7 receivers

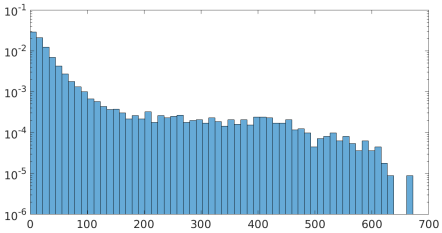

(a) Error distribution with 1 Hz resolution and 4 receivers

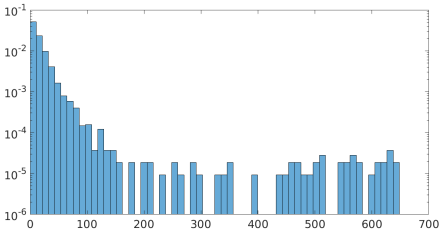

(b) Error distribution with 1 Hz resolution and 7 receivers

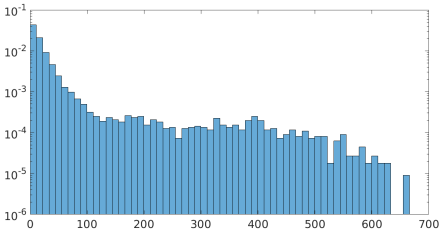

(c) Error distribution with 0.125 Hz resolution and 4 receivers

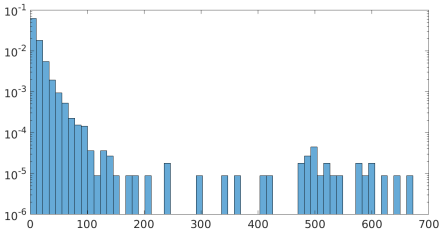

(d) Error distribution with 0.125 Hz resolution and 7 receivers

Figure 15. Errors in distance estimation [km]

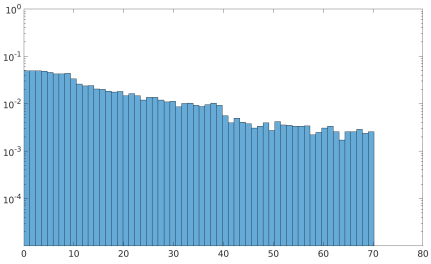

(a) Error distribution with 1 Hz resolution and 4 receivers

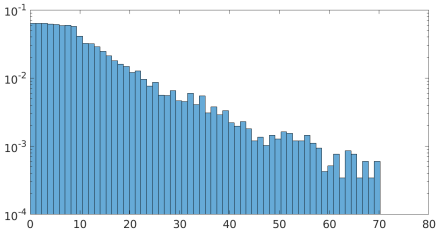

(b) Error distribution with 1 Hz resolution and 7 receivers

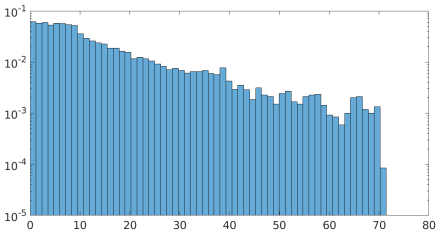

(c) Error distribution with 0.125 Hz resolution and 4 receivers

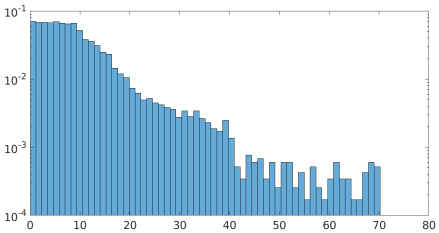

(d) Error distribution with 0.125 Hz resolution and 7 receivers

Figure 16. Errors in speed estimation [knot]

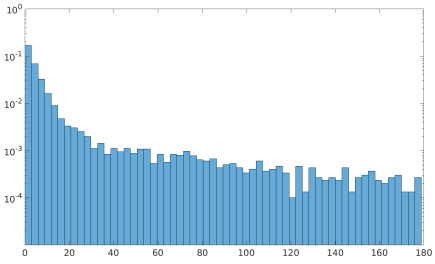

(a) Error distribution with 1 Hz resolution and 4 receivers

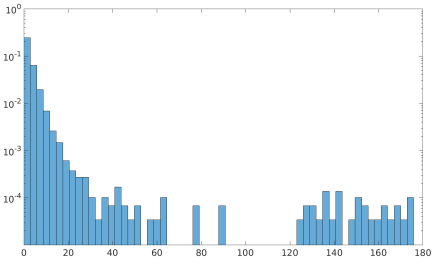

(b) Error distribution with 1 Hz resolution and 7 receivers

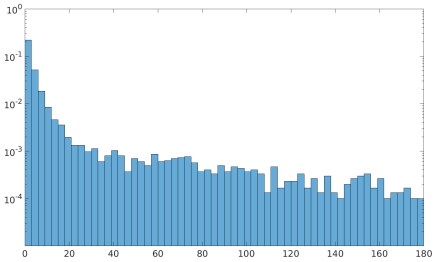

(c) Error distribution with 0.125 Hz resolution and 4 receivers

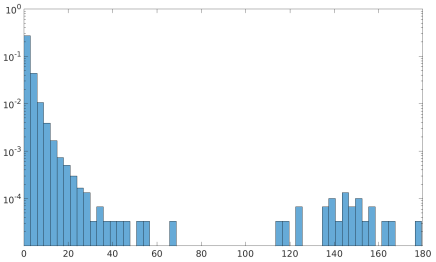

(d) Error distribution with 0.125 Hz resolution and 7 receivers

Figure 17. Errors in bearing estimation [degree]

4.1.2 Maximum Likelihood Estimation

In this section, the possible improvement over variables by Maximum Likelihood Estimation is studied. The results from nearest neighbor search were used as initial guess in MLE. In order to measure the efficiency of MLE, the results were compared to results from the nearest neighbor search. Figures 18, 19 and 20 illustrate the difference between results from nearest neighbor search and MLE. Positive values in figures represent the improvement over the initial guess. Negative values represent deterioration in the estimation of the initial parameters.

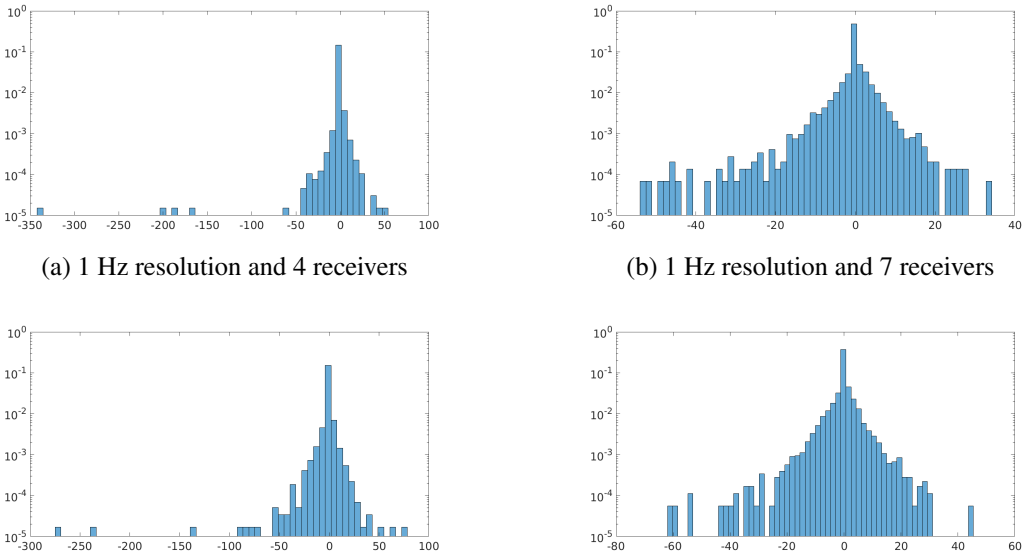

(a) 1 Hz resolution and 4 receivers

(b) 1 Hz resolution and 7 receivers

(c) 0.125 Hz resolution and 4 receivers

(d) 0.125 Hz resolution and 7 receivers

Figure 18. Change of errors in distance estimation [km]

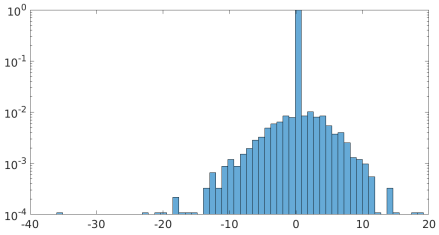

(a) 1 Hz resolution and 4 receivers

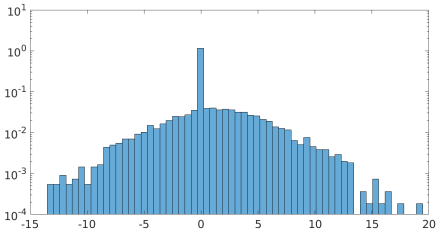

(b) 1 Hz resolution and 7 receivers

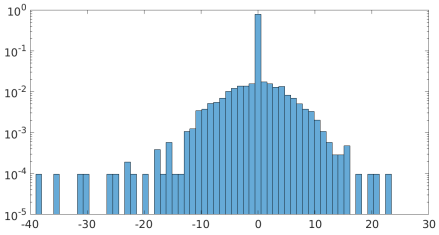

(c) 0.125 Hz resolution and 4 receivers

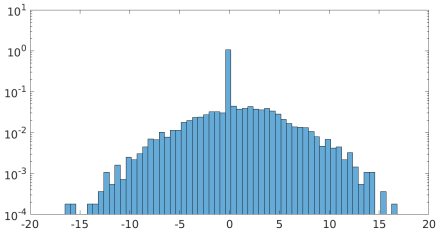

(d) 0.125 Hz resolution and 7 receivers

Figure 19. Change of errors in speed estimation [knot]

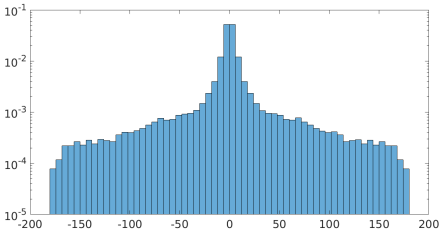

(a) 1 Hz resolution and 4 receivers

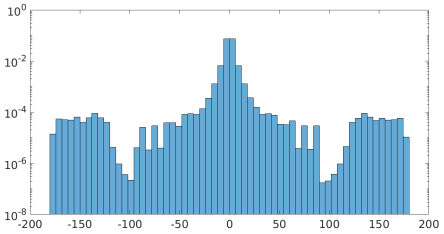

(b) 1 Hz resolution and 7 receivers

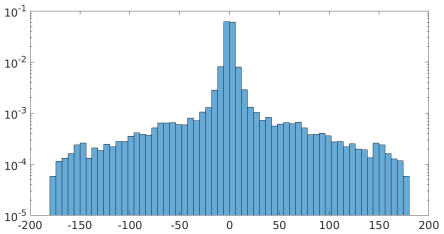

(c) 0.125 Hz resolution and 4 receivers

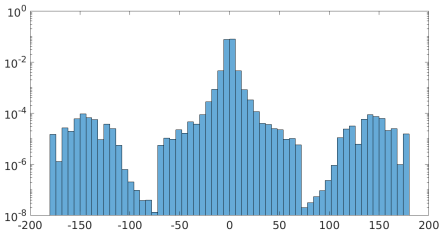

(d) 0.125 Hz resolution and 7 receivers

Figure 20. Change of errors in bearing estimation [degree]

4.2 Experimental Results

In this section, we estimated the initial parameters of real aircraft detected by our receivers. Nine observed days between 9 January 2018 and 15 February 2018 were chosen to process. The minimum number of receivers at the time of initialization is chosen to be 4, as explained in Section 3.1. The receivers made the observations with 1 Hz resolution. The observed Doppler shifts during the time of initialization were passed to lookup table and their corresponding nearest neighbors were calculated according to Section 3.2. ADS-B information were also recorded and used to measure the performance of the experimental setup.

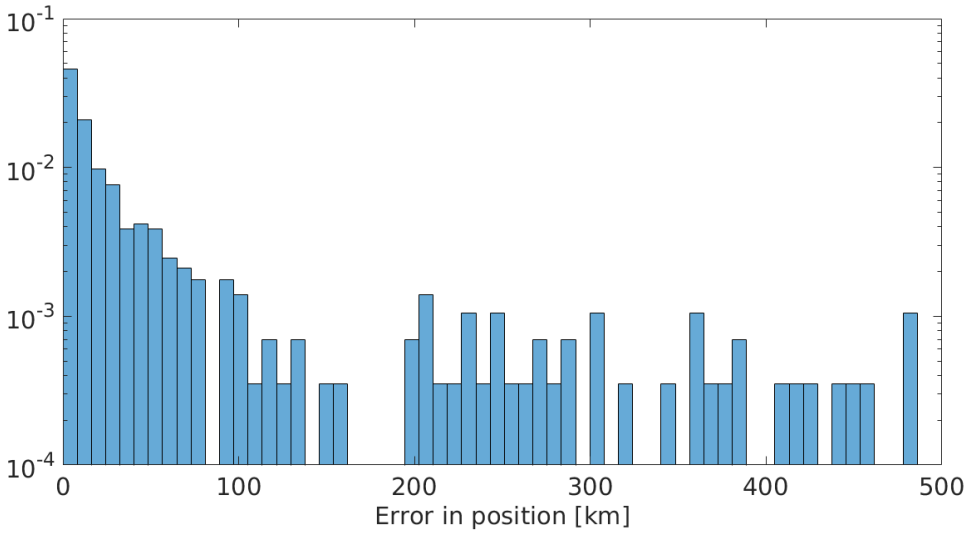

Figure 21. Errors in distance estimation [km]

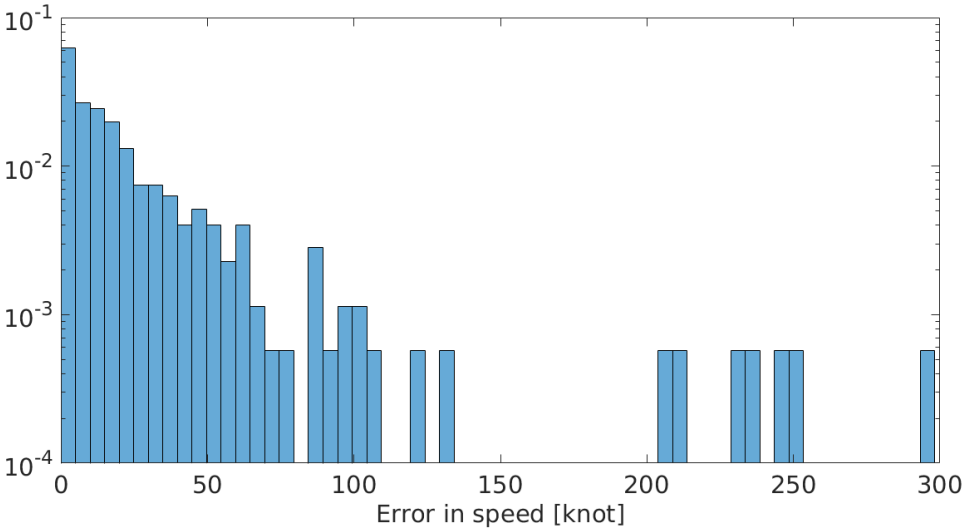

Figure 22. Errors in speed estimation [knot]

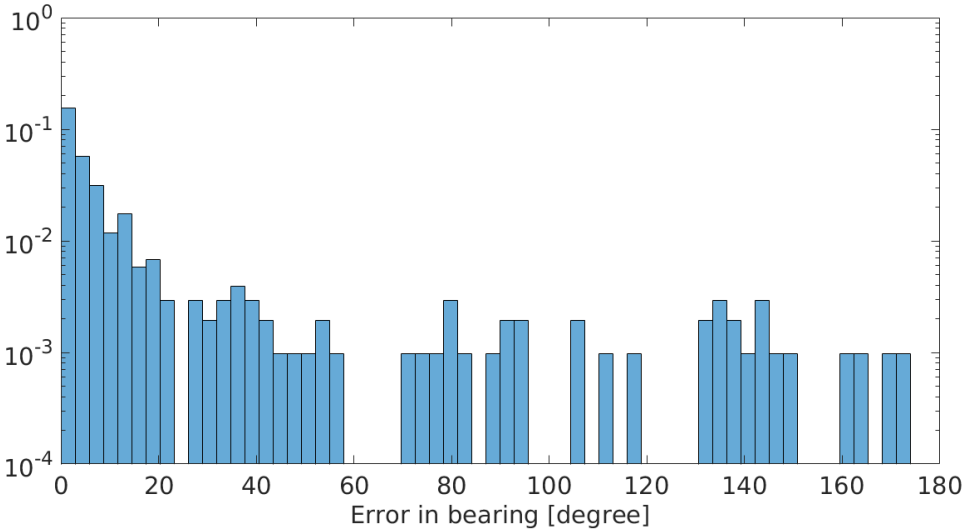

Figure 23. Errors in bearing estimation [degree]

5 DISCUSSION

We have evaluated the performance of two algorithms that initialize an independent passive multistatic radar. The first algorithm detects Doppler curves that are caused by aircraft in the radio signal data. The second one optimizes the initial parameters of the Extended Kalman Filter.

The performance of the first algorithm has been analyzed by the real data that is recorded by our experimental setup. The aircraft that fly through the area, which is covered by our receivers, for a significant time have caused a long enough Doppler curves to be detected. The algorithm has succesfully detected their curves and initiated the tracking. We also successfully followed their curves over short or long observational gaps. The algorithm has also given a number of false detections (false positive) due to random noise in the RSD. Furthermore, we noted that a polynomial fit for the long gap fails to represent the shape of the Doppler curve in some unusually high maneuvering aircraft. Overall, the algorithm to identify the Doppler curves in RSD performed well.

The performance of the second algorithm has been analyzed both the real and simulated data and these tests provided an insight about the capabilities of the experimental setup. According to simulation results, initial state estimation with 7 receivers is clearly better than the one with 4 receivers in every parameter (Figure 11-17). However, this is not a realistic scenario since not every aircraft can be observed by the all of the receivers. The initial state estimation with 4 receivers produced results in acceptable accuracy for the most of the samples. Moreover, tracking with 4 receivers is expected to trigger the algorithm earlier than tracking with 7 receivers, given that aircraft can be detected by 7 receivers. The simulation results also demonstrated that there is a significant improvement in the accuracy with the higher resolution. The Maximum Likelihood Estimation method failed to deliver any meaningful contribution.

The results of the experimental tests with 4 receivers and 1 Hz resolution agree with the simulation test results. We did not seek any further improvements in the state estimation by MLE, as we have seen in the simulation tests that it failed to do so.

The algorithms have been developed considering the flight characteristics of commercial airplanes. We have assumed that the Doppler curves we aim to identify are smooth curves as shown in Figure 4. Irregular curves with frequent twist that can be caused by high maneuvering targets may not be followed by the first algorithm since they cannot be fitted by low-order polynomials. The lookup table for the nearest neighbor search was

constructed with a small range of speed values that would be reasonable for commercial airplanes. A target whose speed is not in this range would not be initialized properly for the Extended Kalman Filter. Last but not least, we assumed that there is only one target available at a time. Multi-target tracking is left for future work.

6 CONCLUSIONS

The purpose of this work was to develop an independent system to initialize tracks for a passive radar. Two algorithms were developed to achieve this objective. The first algorithm analyzes the radio signal data and identifies the Doppler curves that are caused by aircraft. The second algorithm estimates the initial state of the aircraft and initiates the tracking by the Extended Kalman Filter. As a result, an online and stand-alone passive radar, which is independent from ADS-B or human assistance, can be constructed.

The second algorithm was founded on the nearest neighbor search algorithm. The flight characteristics of commercial airplanes were determined from the historical data and they were used to generate the lookup table. Estimating the initial state of the target by historical data is not a common technique that is used by the passive radar community. This work clearly demonstrates that it is a viable option for targets with predictable trajectories.

The equipment used in the experimental setup is relatively cheaper, more mobile and less visible than that of the conventional radar systems. This would allow for civilian application as well as military applications. Receivers can be deployed easily in urban areas if extra radar coverage is needed or almost invisible military surveillance can be set up.

6.1 Future Work

The research presented in this thesis has some restrictions as discussed in Section 5. We suggest the following future extensions to our work:

1. Making the algorithm that identifies the Doppler curves follow any kind of curve so that high maneuvering targets can be identified.
2. A method to determine if flight characteristic of the target does not match the those in the lookup table.
3. An auxiliary method for the cases that lookup table fails.
4. Adding multi-target tracking feature.

REFERENCES

[1] Merrill I Skolnik. *Introduction to radar systems*. McGraw-Hill, 2 edition, 1981.

[2] Federal Aviation Association. *ADS-B Broadcast Services*. 2014.

[3] Rasim Akin Sevimli. Target detection and imaging on passive bistatic radar systems. Master's thesis, Bilkent University, 2014.

[4] P. Ptak, J. Hartikka, M. Ritola, and T. Kauranne. Long-distance multistatic aircraft tracking with vhf frequency doppler effect. *IEEE Transactions on Aerospace and Electronic Systems*, 50(3):2242–2252, July 2014.

[5] P. Ptak, J. Hartikka, M. Ritola, and T. Kauranne. Aircraft classification based on radar cross section of long-range trajectories. *IEEE Transactions on Aerospace and Electronic Systems*, 51(4):3099–3106, Oct 2015.

[6] P. Ptak, J. Hartikka, M. Ritola, and T. Kauranne. Instantaneous doppler signature extraction from within a spectrogram image of a vhf band. *IEEE Transactions on Aerospace and Electronic Systems*, 52(2):576–589, April 2016.

[7] Piotr Ptak. *Aircraft tracking and classification with VHF passive bistatic radar*. PhD thesis, Lappeenranta University of Technology, 2015.

[8] M. Tolonen, P. Ptak, J. Hartikka, M. Ritola, A. Ludvig, M. Korhonen, and T. Kauranne. Forward-scatter doppler-only commercial airliner tracking. In *2017 18th International Radar Symposium (IRS)*, pages 1–8, June 2017.

[9] Eleni Adrian. Doppler effect, 1995.

[10] Mark Richards. *Fundamentals of Radar Signal Processing*. McGraw-Hill, 2005.

[11] Greg Welch and Greg Bishop. *An Introduction to the Kalman Filter*. University of North Carolina at Chapel Hill Department of Computer Science, Chapel Hill, NC, first edition, 2001.

[12] Petteri Aimonen. *Basic concept of Kalman filtering*. 2011.

[13] Garry Einicke. *Smoothing, Filtering and Prediction*. 2012.

[14] M. Linderoth, K. Soltesz, A. Robertsson, and R. Johansson. Initialization of the kalman filter without assumptions on the initial state. In *2011 IEEE International Conference on Robotics and Automation*, pages 4992–4997, May 2011.

[15] J. A. Nelder and R. Mead. A simplex method for function minimization. *The Computer Journal*, 7(4):308–313, 1965.